Determination of particle number concentration for biological particles using AF4-MALS: Dependencies on light scattering model and refractive index

Christine L. Plavchak,[1] *Allison Z. Werner,*[2] *Elizabeth Betz,*[1] *Davinia Salvachúa,*[2] *Gregg T. Beckham,*[2] *and S. Kim Ratanathanawongs Williams*[1] *

[1]Department of Chemistry, Colorado School of Mines, 1500 Illinois St., Golden, Colorado, 80401, United States

[2]Renewable Resources and Enabling Sciences Center, National Renewable Energy Laboratory, Golden, Colorado, 80401, United States

*Corresponding author

Email: krwillia@mines.edu

"For Table of Contents Only"

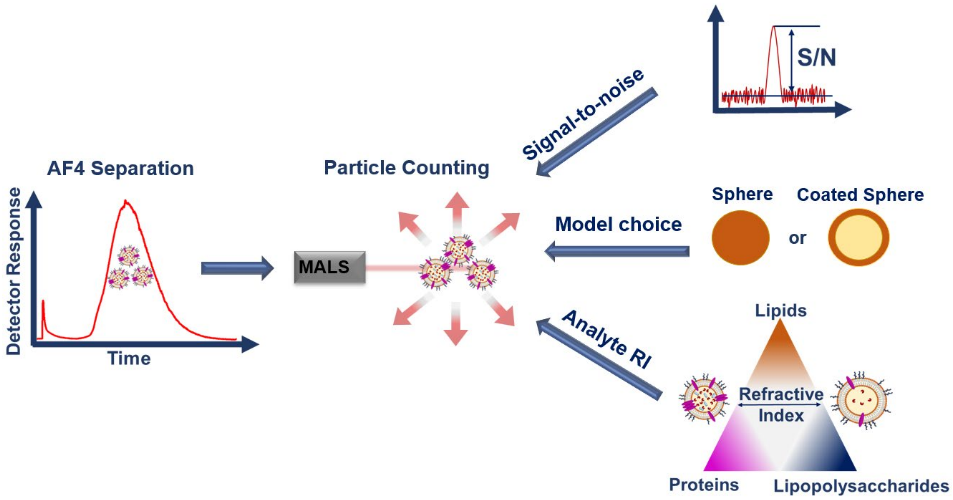

ABSTRACT:

Determining accurate counts and size distributions for biological particles (bioparticles) is crucial in wide-ranging fields, but current ensemble methods to this end are susceptible to bias from polydispersity in size. This bias can be mitigated by incorporating a separation step prior to characterization. For this reason, asymmetrical flow field-flow fractionation (AF4) with on-line multiangle light scattering (MALS) has become an important platform for determining particle size. AF4-MALS has been used to report particle concentration, particularly for complex biological particles, yet the impact of light scattering models and particle refractive indices (RI) have not been quantitatively assessed. Here, we develop an analysis workflow using AF4-MALS to simultaneously separate and determine particles sizes and concentrations. The impacts of the MALS particle counting model used to process data and the chosen RI value(s) on particle counts are systematically assessed for polystyrene latex (PSL) particles and bacterial outer membrane vesicles (OMVs) in the 20-500 nm size range. Across spherical models, PSL and OMV particle counts varied up to 13% or 200%, respectively. For the coated-sphere model used in the analysis of OMV samples, the sphere RI value greatly impacts particle counts. As the sphere RI value approaches the RI of the suspending medium, the model becomes increasingly sensitive to the light scattering signal-to-noise ultimately causing erroneous particle counts. Overall, this work establishes the importance of selecting appropriate MALS models and RI values for bioparticles to obtain accurate counts and provides an AF4-MALS method to separate, enumerate, and size polydisperse bioparticles.

INTRODUCTION

The measurement of physicochemical properties of polydisperse, complex biological particles (bioparticles) is an essential step towards understanding their function and harnessing their properties. Characteristics such as size and particle concentration are key attributes yet there lacks a standardized way to measure and report these values among different research areas. While much attention has focused on developing reproducible and accurate sizing techniques for < 500 nm diameter particles, lesser attention has been given to particle counting until recently.

This interest has been driven by the realization that bioparticles can play important roles in processes such as cell-cell signaling via exosomes[1], function as biomarkers[2,3], and be used as therapeutic tools.[4] In these scenarios, particle size distribution and concentration are important primary characteristics that are relatable to observed function, stability, potency, and batch-to-batch or biological reproducibility.

Multiple orthogonal techniques rooted in different principles have been used to determine particle size and/or concentrations of extracellular vesicles, lipid nanoparticle drug carriers, etc.[5] Current ensemble methods include tunable resistive-pulse sensing (TRPS)[6], Coulter counter (CC)[7], dynamic light scattering (DLS)[8], flow cytometry (FC)[5], nanoparticle tracking analysis (NTA)[9], and multiangle light scattering (MALS).[10] However, ensemble methods such as these only provide averages and do not capture information regarding size distributions within the sample. Further, TRPS, CC, and FC are not sensitive enough to analyze small particles (e.g., < 30 nm in diameter) and all methods except for FC often cannot readily accommodate large particle size distributions within a sample set (e.g., 20-500 nm). The latter is because of either instrumental constraints (e.g., needing multiple apertures (CC), buildup of particles around tunable pores (TRPS), camera setting sensitivities (NTA)) or larger particles disproportionately impacting light signal intensities (MALS).

Particle separation can mitigate ensemble biases by creating more monodisperse sample subpopulations prior to sizing and quantifying. Two of the techniques mentioned previously, NTA and MALS, have been coupled to size exclusion chromatography (SEC) and asymmetrical flow field-flow fractionation (AF4) and NTA has been also been utilized as an offline, post-fractionation counting technique.[11–13] NTA estimates particle size and count by optically tracking the Brownian motion of particles in solution; however, the results of NTA measurements are often influenced by instrumental parameters.[14,15] MALS measures the light scattering intensity from particles at different known angles and fits these intensities to light scattering formalisms or shape-specific models to obtain size and count information. Incorrect use of the formalisms or shape-specific models, however, may introduce significant errors in reported values such as molar mass, size, and particle count.[16]

AF4-MALS has been increasingly used to determine particle concentration particularly for bioparticles such as virus-like particles, lipid-based nanocarriers,[5,10,17–19] and extracellular vesicles.[20–22] In the absence of certified particle standards, comparisons between multiple techniques are the means to a better understanding of methodological robustness and accuracy.[5,12,23] Comparisons with AF4-MALS have not examined the impact of accurate analyte parameters and data processing (e.g., refractive index values and light scattering model, respectively) on the reported particle concentration and warrants additional investigation.

To address this knowledge gap, an analytical AF4-MALS method suitable for dilute sample suspensions of 20 nm to ~500 nm size particles was developed. The effect of light scattering model and refractive index on particle counts was then systematically evaluated for polystyrene latex (PSL) standards and bacterial outer membrane vesicles (OMVs). OMVs were chosen as an exemplary bioparticle for this study as they are polydisperse (e.g., 25 to 500 nm[24–26]) and have a core-shell structure with a varying shell composition based on differing ratios of lipoproteins, phospholipids and proteins,[27] all of which affect RI. The AF4-MALS method we present provides simultaneous size-based separation and particle concentration of PSL standards and OMVs. Overall, this study provides foundational knowledge necessary to acquire accurate bioparticle counts via MALS and presents an AF4-MALS method for the separation and enumeration of bioparticles such as bacterial OMVs.

MALS PARTICLE COUNTING THEORY

The basic principles of MALS originate from fundamental equations defined by Maxwell[28], then later simplified by Rayleigh in the case of particles with a radius less than one tenth of the wavelength of radiation. The Rayleigh-Gans Debye (RGD) approximation was developed as an extension of Rayleigh's original theory to better understand light scattering for larger macromolecules, yet still contained some size limitations and assumptions that will be discussed in the following section.[29,30] To overcome this, the Mie theory was developed to rely on the exact mathematical solutions to Maxwell's equations for a spherical particle interacting with polarized light.[31] A more detailed explanation of these two theories are described elsewhere.[32,33] Regarding the use of these theories for particle counting, there are subtle differences in their particle counting equations[34,35] and it is important to understand the assumptions for data analysis and interpretation.

Mie Theory

The use of MALS as a particle sizing and counting technique is based on measuring the light scattering intensities at different angles.[16] Depending on the size of the analyte of interest, more intense scattering can be measured at the lower, more forward detectors (< 90°) thus giving rise to some angular dependence in measuring particle size. The intensity of scattered light from a spherical particle for measurements made in the θ plane with incident light polarized perpendicularly and at some known angle can be represented as:

$$I_{\theta S} = \frac{I_o N \Delta v}{(kr)^2} i(\theta) \tag{1}$$

where N is the total number of particles/mL, Δv is a pre-determined scattering volume, $k = 2\pi n_o / \lambda_o$ where n_o is the refractive index of the solvent and λ_o is the wavelength of the laser, r is the length to the detector, and $i(\theta)$ is the differential intensity or single particle scattering function (**Eq. 2)**. The most important analyte-dependent parameters in **Eq. 2** are the volume of the sphere or size (V), the refractive index of the analyte (n_a), and form factor ($P(\theta)$).

$$i(\theta) = \left(\frac{1}{4\pi}\right) k^6 V^2 \left(\frac{n_a}{n_o} - 1\right)^2 P(\theta) \qquad (2)$$

To solve for *N***, Eq. 1** can be substituted into the Rayleigh ratio ($R(\theta) \propto I_{\theta S}/I_0$) and simplified leading to the following equation:

$$N = \frac{k^2 R(\theta)}{i\,(\theta)} \qquad (3)$$

It is shown in **Eq. 3** that the particle count is impacted by the measured light scattering intensity, but inversely proportional to the analyte-dependent parameters mentioned above. The angular dependence on particle size and the incorporation of size into **Eq. 2** suggests that the measured light scattering intensities and detector selection during data analysis may be a crucial component in data analysis. Particle counting using Mie theory can be applied to particles spanning a range of 20-500 nm in diameter (depending on instrumental limitations)[34], but the reliability of using this model is greatly influenced by RI values.

Rayleigh-Gans-Debye (RGD) Approximation

While Mie theory is modeled as a direct solution to light interacting with a spherical particle, the RGD approximation is ideally satisfied by measuring the light scattering intensity at the 0° scattering angle. The relationship of the scattered light intensity, concentration, and molar mass is simple at this angle, yet measuring the intensity at that location is impossible due to the placement of the MALS laser. To overcome this, experimental data is typically extrapolated back to the 0° during data analysis and the use of lower angles closer to 0° can be critical in assessing accuracy of the measurement for size and molar mass.[16] For the RGD approximation, it is known that:

$$\frac{K^{*}c}{R(\theta)} \approx \frac{1}{M_w(P(\theta))} \text{ where } K^{*} = \frac{4\pi^2 {n_0}^2}{N_A {\lambda_0}^2}\left(\frac{dn}{dc}\right)^2 \quad (4, 5)$$

Where $R(\theta)$ is the Rayleigh ratio, c is the analyte concentration, M_w is the molar mass of the analyte, $P(\theta)$ is the form factor, and K^* contains the refractive index of the solvent (n_o), dn/dc of the analyte, and wavelength of the laser (λ_0). If the limit $\theta \to 0$ is considered, then $P(0) = 1$. Inserting this value into **Eq. 4,** the RGD approximation can be rewritten as:

$$R(0) \approx K^{*}c\, M_w \approx K^{*}n_i\, M_i^2 \quad (6)$$

The concentration can be considered as $c = n_i\, M_i^2$ and assuming the analyte has a mass (M_i), can occupy a volume (V_i) and thus a uniform density (ρ) so that $\rho = M_i/V_i$. If this holds true, the following proportionality can be made:

$$N \propto \frac{R(0)}{V_i^2} \quad (7)$$

The upper size limit for using the RGD approximation is roughly 100 nm in diameter, prohibiting the use of the RGD approximation for a more polydisperse sample (20-500 nm)[36]. It is also important to note the assumptions for **Eqs. 3 and 7** are the following: 1) particles are monodisperse in size, 2) there are zero contributions of scattering from solvent, giving an absolute Rayleigh ratio (R(θ)) ($R(\theta_i) = R_s(\theta_i) - R_f(\theta_i)$ where θ_i = known angle, R_s= Rayleigh ratio of the solution and R_f = Rayleigh ratio of carrier fluid), 3) real and imaginary refractive index (RI) values are known, and 4) the RGD approximation can be used when particle refractive index is close to the RI value of the suspending fluid ($n_a/n_o - 1 \ll 1$). [35,37]

MALS Particle Count Models

Sphere models for particle counting are the focus of this work. Three different spherical models can be used to analyze particles and the underlying theories that they are formed from follow either Mie theory or the RGD approximation. The “Lorenz-Mie” and “coated sphere” models use Mie theory while “sphere” model uses the RGD approximation.

To successfully use these models, all three require sphere radius information which can be determined by online MALS along with the analytes’ absolute and imaginary RI values. The sphere and Lorenz-Mie models require only one RI value whereas the coated sphere model needs two RI values (sphere and shell RI) and knowledge of the shell thickness.

EXPERIMENTAL SECTION

Materials and Methods

Duke polystyrene latex (PSL) particles with sizes of 22, 100, and 496 nm (Thermo Fisher Scientific, Waltham, MA) were used in the AF4 method development and were suspended in 0.02% sodium azide (Sigma-Aldrich, St. Louis, MO) and 0.05% FL-70 surfactant (Thermo Fisher Scientific, Waltham, MA) in deionized 18.2 MΩ·cm water for the carrier fluid. For OMV separation, 150 mM phosphate buffered saline (PBS) was prepared with sodium chloride (Thermo Fisher Scientific, Waltham, MA), potassium chloride (Mallinckrodt Chemical, St. Louis, MO), sodium phosphate dibasic (Thermo Fisher Scientific, Waltham, MA), and potassium phosphate monobasic (Mallinckrodt Chemical, St. Louis, MO).

Production and isolation of OMVs

Pseudomonas putida KT2440 (*P. putida)* was inoculated into 50 mL of M9 minimal media (6.78 g/L Na_2HPO_4, 3 g/L KH_2PO_4, 0.5 g/L NaCl, 1 g/L NH_4Cl, 2 mM $MgSO_4$, 100 µM $CaCl_2$, and 18 µM $FeSO_4$) supplemented with 5 g/L glucose ("lignin-free" condition) or 5 g/L glucose plus 25% (v/v) alkaline liquor from corn stover pretreatment with NaOH ("lignin-rich" condition) in biological triplicate. These cultivation conditions were selected based on a previous study that suggested that OMV sizes depend on the media composition.[38] All chemicals other than 'the lignin-rich' liquor, which was made in-house as has been described previously,[39] were purchased from Sigma-Aldrich (St. Louis, MO). Cultivation conditions and OMV isolation and purification were performed as previously described.[38]

Asymmetrical flow field-flow fractionation (AF4) and multi-angle light scattering (MALS)

All experiments were performed using an AF2000 system (Postnova Analytics, Salt Lake City, UT) coupled to a SPD-20A UV/Vis detector (Shimadzu, Columbia, MD), multi-angle light scattering (MALS) DAWN HELEOS II (Wyatt Technology Corporation, Santa Barbara, CA). The channel was formed with a tip-to-outlet length of 27.5 cm, breadth at channel inlet of 2 cm, breadth of channel outlet of 0.5 cm, and a spacer with a nominal thickness of 350 µm. The accumulation wall was a 30 kDa molecular weight cutoff regenerated cellulose membrane (Postnova Analytics, Salt Lake City, UT). A 0.1 µm inline filter (Merck Millipore Ltd, Darmstadt, Germany) between the HPLC pump and the AF4 channel was used to filter 0.02% sodium azide and 0.05% FL-70 surfactant along with 150 mM PBS as the two carrier fluids used in this study.

The initial AF4-UV-MALS method had a focusing time of either 10 or 15 minutes, the injection flow rate was 0.2 mL/min, the detector flow rate was 0.5 mL/min, and the sample injection volume was either 200, 500, and 1000 µL. The crossflow rate was programmed to start at 1.0 mL/min during focusing, then decreased linearly to 0.1 mL/min over 10 minutes, held at 0.1 mL/min for 20 minutes, and then turned off. For OMV fractionation, the isocratic hold at 0.1 mL/min was shortened to 2.5 minutes after testing the methods with the different OMV samples used in this study.

Particle Counting Analysis using MALS

Data acquisition and particle counting analysis were performed using ASTRA 7.3.2.21 (Wyatt Technology Corporation, Santa Barbara, CA). The MALS detector was normalized using bovine serum albumin (BSA) (Sigma-Aldrich). For each PSL size, triplicate runs were injected into the AF4 using a 200 µL sample loop and the AF4 method described in the previous section. The 22 and 100 nm PSL particles were diluted by 200, 400, 1,000, or 2,000x and 90% of the MALS laser power was used. The 496 nm particles were diluted by 1,000, 2,000, 4,000, and 8,000x and the MALS laser power was set to 25% to prevent saturation of the low-angled detectors (detectors 1-8). Using the ASTRA software, the sphere and Lorenz-Mie models and RI = 1.58 for PSL were used. Detectors 2-18, 5-18, and 9-18 were used for the 100 and 496 nm PSL. Corresponding detector angles can be seen in **Table S2.**

For OMV particle counting, the MALS laser power was set to 90%, and ‘Heavy’ was chosen as the despiking level for the MALS signal. In addition to the sphere and Lorenz-Mie models used in the PSL analysis, the coated sphere model was also examined. A RI range of 1.35-1.65 was used to encompass the varying composition of the OMVs. Detector selection was determined by examining the best R^2 value at the peak maximum for each sample. For lignin-free samples, detectors 8-17 were selected while detectors 7-17 were chosen for the lignin-rich samples.

Additional details regarding the RI range and detector selection and will be discussed more in the following section.

For both PSL and OMVs, the number of particles were obtained from the summary report from the ASTRA software. The particle concentration or number of particles per milliliter was obtained using the volume of the analyte peak. The volume was determined from the area under the peak multiplied by the detector flow rate.

RESULTS AND DISCUSSION

AF4-MALS Method for Size-Based Separation and Enumeration

Adaptation of AF4 Method with PSL Standards

Current AF4 separations for bioparticles or macromolecules use injection volumes that span 10-150 µL.[40,41] While these volumes are suitable for characterization, they may not be suitable for fraction collection and further offline analyses due to significant sample dilution. This may also lead to low light scattering intensities thereby impacting size and count analysis.[5] To increase the measured light scattering intensity and decrease the number of AF4 runs needed to produce sufficient quantities of subpopulations for further analysis, injection volumes of 200, 500, and 1000 µL were investigated. A PSL mixture of 22, 100, and 496 nm particles was chosen due to the size range of the bacterial OMVs (25-500 nm). Experiments contained the same sample mass, which was adjusted to accommodate the larger injection volumes, and retention time and sample recovery were evaluated across the different sample loops.

As injection volume increased, consistent retention times and peak areas were observed for each species in the PSL mixture showing successful separations (**Figures 1 and S1**). Sample recovery, assessed by comparing the UV peak areas of the separated mixture (or with crossflow) from the area of the peak observed without the crossflow (**Figure S1**), was slightly higher than the accepted sample recovery of >70% across the three sample volumes.[42] For the 22, 100, and 496 nm PSL standard mixture, the total sample recovery was estimated to be 81, 83, and 75% for the 200, 500, and 1000 µL loops, respectively. Thus, the AF4 method used here is amenable to scale-up without significantly reduced sample recovery, and therefore 1000 µL was used for separation of the OMVs to maximize the amount of sample processed per run.

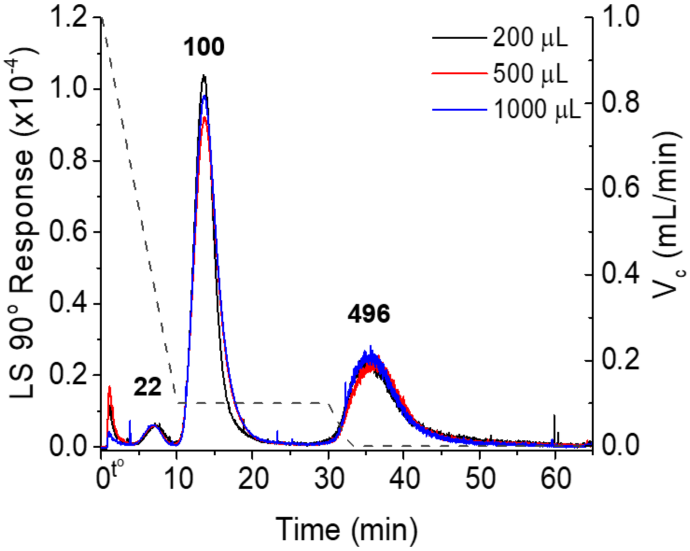

Figure 1. AF4-MALS separation of a 22, 100, and 500 nm polystyrene latex mixture using 200, 500, and 1000 µL sample loops. The dashed line and right y-axis show the crossflow rate program.

MALS Particle Counting: Utilization of Spherical Models with PSL Standards

To understand the limitations (model, particle size, etc.) associated with MALS particle counting, it was of interest to utilize the PSL standards used in the AF4 method development for particle counting. Expanding beyond the AF4 method, PSL has a known spherical shape and well-known RI value (1.58). Currently there is no absolute count standard (< 1 µm) or count standard for biological particles, which would provide a better model for assessing MALS particle counting for OMVs. As discussed in the MALS Particle Counting Theory section, the sphere and Lorenz-Mie models can be used to examine spherical particles. Since the 100 nm PSL particles are at the upper limit of the sphere model, this size was used to examine changes in particle count between the two models. The 22 nm PSL sample could not be fit to either the sphere or the Lorenz-Mie models. This could be due to the lower size limitations of the MALS or the lower light scattering signal of this species. The Lorenz-Mie model could only be utilized for the 496 nm PSL because of that upper size limitation of the RGD approximation. Two additional assumptions are considered: PSL stock solutions are 1% solids based on the manufacturer's certification of analysis (CoA) and 100% recovery is achieved in the AF4 separation. Based on this estimated value and diameter of the particle, one can calculate a particle count using **Eq. 8**, where $W_v\%$ is the percent solids based on the CoA, ρ_p is the polymer microsphere density, and D is the diameter of the particle.

$$N_p = \frac{W_v\% \times 6x10^{10}}{\pi \rho_p D^3} \tag{8}$$

Experimental particle counts compared to nominal values for the 100 nm PSL are shown in **Figure 2.** Both the sphere and Lorenz-Mie models have linear trends with good R^2 values (0.999). This linear trend demonstrates that we see the appropriate response to changes in particle counts with an increase in injected sample concentration and suggests that if the calculated particle count was accurate and 100% sample recovery was achieved and there is no aggregation of the analyte[43], the slope of the line would reach unity. Between the two models, the Lorenz-Mie model has consistently larger particle counts compared to the sphere model by 11-12%, raising the question as to which is the more accurate model.

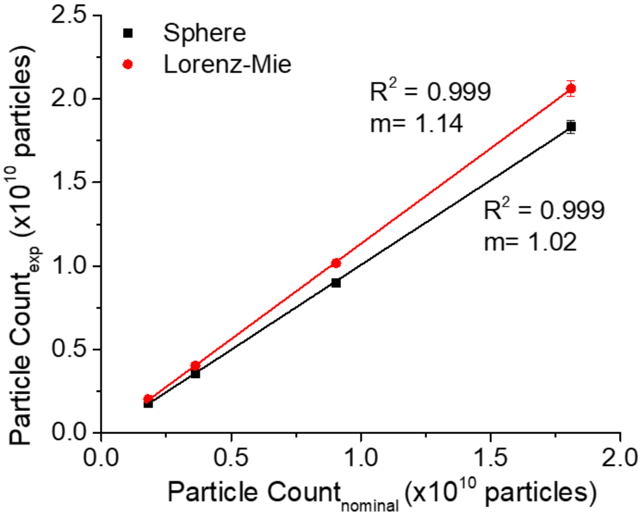

Figure 2. Comparison of experimental and nominal particles counts using the sphere and Lorenz-Mie models for PSL standards. The nominal counts are based on a 200 µL injection volume and 1% solid suspension of 100 nm PSL. Detectors 5-18 were used in this analysis.

One contribution to this consistent difference between the two models could lie within the measurement of the particle size or volume. In both **Eqs. 2 and 7,** the volume is a squared term, and inversely proportional to the number of particles per milliliter. Upon further investigation, online radius data showed minimal differences in size or changes in the uncertainty in the measurement (< 2 %). The other potential reasoning for this consistent difference is centered around the assumption $(n_a/n_o - 1 \ll 1)$. While the RI value for PSL is known (1.58), the differences in particle count values between the two models can be examined by changing the RI value for PSL during data analysis. **Figure 3** shows an increasing percent difference between the two models as the analyte's RI increases. Between RI values of 1.55 and 1.6, the percent difference ranges between 10.1 and 13.3 %, correlating to differences seen in **Figure 2.** This suggests that the Lorenz-Mie model may be a more well-suited model for samples with higher RI values.

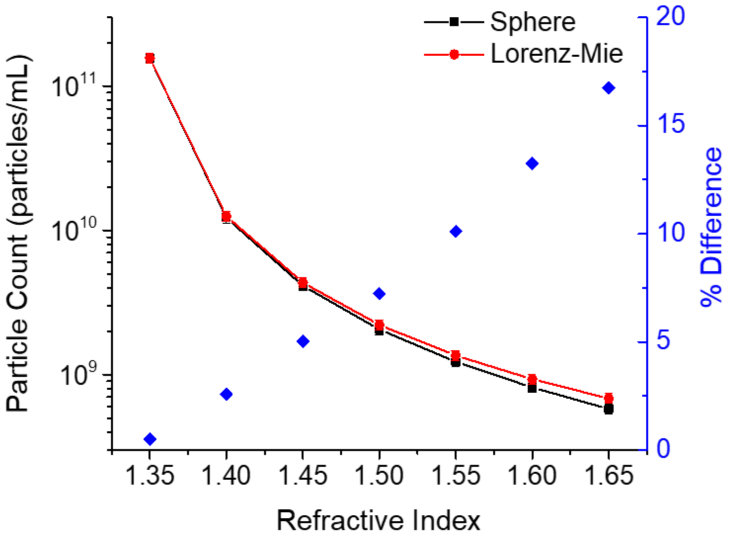

Figure 3. Changes in particle concentration as a function of refractive index for 100 nm PSL particles using the sphere and Lorenz-Mie models.

In addition to the two different models, another component of data processing is the selection of the different MALS detectors during the analysis. It is suggested that the smaller angles should be selected during data analysis to better satisfy the RGD approximation to help extrapolate the fitted data to the 0° angle. Larger angles may also be selected as it is suggested that the more detectors selected would provide the best representation of the sample.

Effects of selected detectors during analysis of the 100 nm PSL can be seen in **Figure S2.** Three detector ranges were investigated (2-18, 5-18, and 9-18) based on their R^2 values at the peak maximum of the sample. There were no significant changes in particle counts between selecting detectors 2-18 and 5-18 for either sphere or Lorenz-Mie models; however, the fits were drastically different with detectors 2-18 and 5-18 having R^2 values of 0.05-0.07 and 0.6-0.7, respectively. While the smallest angles (detectors 2-4) should satisfy the RGD approximation, they do not contribute to significantly different particle counts due to poor fitting of the analyte to each sphere model. Across the two models there is a difference between the use of detectors 5-18 and 9-18.

This suggests that detectors 5-8 may be crucial to using MALS to calculate particle counts, yet linearity of the data suggests both detector and model choice having significant contributions to changes in experimental counts.

Revisiting the assumptions made for the calculated particle counts in **Figures 2 and S2**, it was assumed that PSL stock is 1% solids. To assess how the slopes of each data set would change if this information was not completely accurate, calculated particle counts assuming 0.8 and 1.2 % solids were investigated. Between the two other sets of nominal counts, the data is still represented linearly, but there is a 22 % increase in slope for assuming 0.8 % solids and 18-19 % decrease in slope for 1.2 % solids (**Figure S3)**. These trends are consistent where 0.8 % solids should have less particles compared to what we see with MALS, therefore a larger slope and the opposite effect with 1.2 % solids.

The 496 nm PSL particles were also examined considering the influences of calculated counts, detector selection and model choice. One major hindrance with a larger-sized population is that because light scatters more in the forward direction and to the diameter to the sixth power, saturation of the lower angled detectors (< detector 8, θ= 64°) is easily achieved at low concentrations. To mitigate this, the laser power of the MALS had to be decreased to 25 %, and lower concentrations had to be utilized. This could make particle counting analysis of large particles, that scatter light more intensely, more challenging. Additionally, because of the larger diameter, only the Lorenz-Mie model could be assessed. Similar to **Figures 2 and S2**, the 496 nm PSL show a linear trend, but with much larger slopes (**Figure S4**). Again, the linear trends suggest that MALS can provide a good correlation between increased concentration and increased particle counts, but absolute particle counts cannot be determined.

Separation and Enumeration of *P. putida* OMVs using AF4-MALS

Size-Based Separation of P. putida OMVs

Given the methodological validation with a polydisperse mixture of PSL standards, we next sought to apply the AF4-MALS method to bioparticles and evaluate the effect of key parameters, such as model and RI, on counts. To generate OMVs, *P. putida* was cultivated in lignin-free or lignin-rich media, and bulk OMVs were harvested at 24 h from biological triplicates. OMVs harvested from both types of media were projected to contain both a small ($\bar{d}$ = 17 and 28 nm) and large ($\bar{d}$ = 120 and 307 nm) OMV populations in lignin-free and lignin-rich cultivations, respectively.[38] For OMV separation, an AF4 method with 1000 µL sample volume was applied to accomplish the following: (i) remove small particles ($d \approx$ 4-6 nm, approximately the size of a single protein) in the focusing step, (ii) elute small OMVs rapidly thereafter, and (iii) elute the large OMVs with intra-population separation.

AF4 separation, MALS signal, and radius were similar for the lignin-rich and lignin-free OMVs (**Figure 4c**). The total OMV populations for lignin-free samples display a lower light scattering signal and a lower size range (d=40-138 nm, both populations) compared to the lignin-rich OMVs (d=32-404 nm, both populations), which is similar yet slightly larger than each anticipated size range.[38] Close alignment between technical replicates demonstrates the AF4 method is reproducible. Within the larger OMV population, the continuous increase in the radius demonstrates intra-population separation is achieved (**Figure 4c**).[29] To the presence and characterize the smaller OMV population (d < 30 nm), AF4 experiments using an isocratic crossflow rate of 0.1 mL/min were completed using the lignin-rich samples (**Figure 4b**). The retention times and MALS signal were then used to calculate the OMV size using AF4 theory to be 20-50 nm in diameter between 1.7 and 3.8 minutes, and particle size was confirmed using batch

DLS (**Figure 4b, shaded region**), confirming the smaller population presence and size. OMV sizes across biological replicates is of interest to understand how size distributions vary. Finally, AF4-MALS was conducted on the biological replicates for both the lignin-free and lignin-rich samples. AF4 retention times, MALS signal (LS 90° Response), and radius distributions were consistent across the triplicates in both media conditions (**Figure 4d** and **4e**). The higher signal-to-noise within the lignin-rich samples is due to the presence of larger particles, as light is scattered ~d^6.

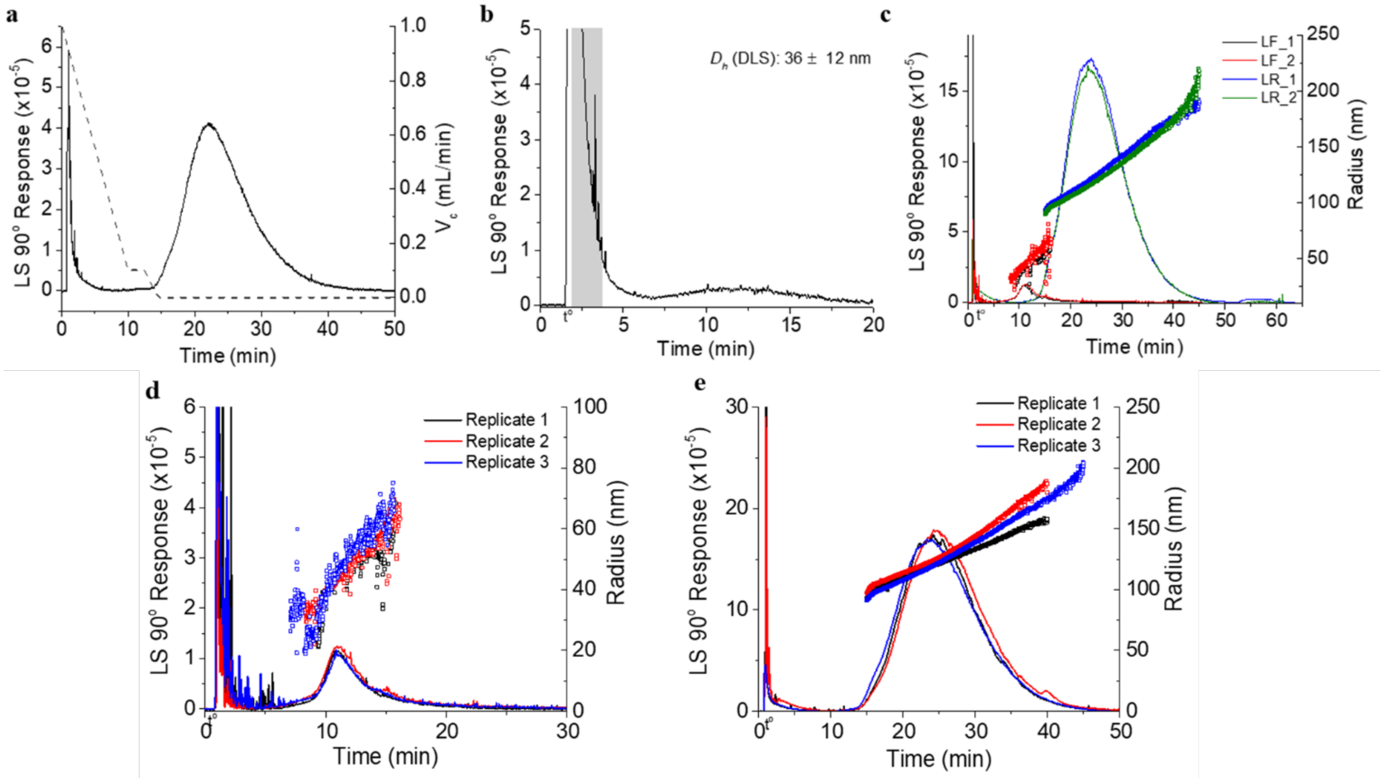

Figure 4. (a) AF4-MALS fractogram of lignin-rich OMVs overlayed with a modified AF4 crossflow program (dotted line) used to fractionate vesicles (b) AF4-MALS fractogram of lignin-rich OMVs separated using an isocratic crossflow of 0.1 mL/min (c) MALS responses and radius distributions across the AF4 separation of *P. putida* OMVs isolated from lignin-free and lignin rich cultivations. Technical duplicates are shown. Reproducibility of three biological replicates of *P. putida* OMVs grown in (d) lignin-free and (e) lignin-rich media. Each MALS fractogram and radius distribution is an average of two AF4 injections. *Estimation of OMV RI Values using the Coated-Sphere Model*

Despite PSL being a simple system to evaluate MALS particle counting, the structure and composition of OMVs are more complex. Thus, how to best represent these vesicles during analysis needs to be considered. The current understanding of *P. putida* OMVs suggests they should be modeled as a core-shell structure: compositionally the shell contains a mixture of lipopolysaccharides (LPS), phospholipids (PL), and transmembrane proteins while the core is filled primarily with water and protein, suggesting the core and shell may have different RIs. One major challenge with examining OMVs and other biological particles is the lack of experimentally determined RI values or methods to easily obtain this information.[44,45] Few studies have utilized experimental data from other techniques like NTA or flow cytometry scatter ratios (Flow- SR) of mammalian EVs to estimate RI values spanning 1.35-1.40.[44] One drawback is that these values may not effectively represent the OMVs used here due to differences in composition.

Taking a more calculated approach, the RI for OMVs could be determined based on the weight percent, partial specific volume of a sphere, and dn/dc values of the individual components to propose how composition changes the overall RI values (**Table S1).**[18] Using this approach, a range of RI values were determined for both the 'shell' and 'core' of the *P. putida* OMVs. For the RI value of the shell, it is understood that there is an LPS and PL bilayer in which transmembrane proteins can embed. Shell RI values were determined for a sliding ratio of LPS, PL, and protein from no protein in the OMV shell (50:50:0 LPS:PL:protein) to having more than half of the surface being protein (20:20:60 LPS:PL:protein). Similarly, core RI values for ranging water:protein content were determined (**Table 1**). Shell and core RIs ranged from 1.49-1.52 and 1.33-1.58, respectively**.** While this range appears to be broad, it encompasses a similar range of RI values determined for mammalian EVs.[46–50] In lieu of having compositional ratios of the OMV components it is important to not only consider how RI changes particle counts, but also how this may affect compositional heterogeneity in these biological systems, discussed in the next section.

Table 1. Calculated dn/dc and RI values for the OMV core-shell structure (coated-sphere model) based on varying composition ratios.

Ratio of LPS: PL: protein	dn/dc (mL/g)	RI Value
50:50:0	0.14	1.49
40:40:20	0.15	1.50
33:33:33	0.16	1.50
20:20:60	0.17	1.52
Ratio of H_2O: protein		
100 :0	-	1.33
80:20	-	1.38
50:50	-	1.46
20:80	-	1.53
0:100	-	1.58

Impacts of RI and LS Model on OMV Particle Counts

After verifying the AF4 separation was reproducible across all biological replicates, and estimated RI values were determined, the impact of RI and light scattering models on particle counts were then examined. While both populations are present, the larger vesicle populations ranging from 8-17 min. (lignin-free) and 15-40 min. (lignin-rich) were used in evaluating the particle count method. The coated sphere model is considered to most closely approximate the OMV structure; additionally, the sphere and Lorenz-Mie models were assessed to identify trends in particle counts and sensitivities in the models. Despite the sphere model having an upper size limit, it was of interest to observe if there were any major changes between the counts determined with sphere and Lorenz-Mie models for the lignin-rich OMVs. Moving forward, the RI values for the "core" of the coated sphere model will be termed "sphere RI."

For lignin-free OMVs, the coated sphere model gives rise to unrealistic particle counts (> 10^{16} particles/mL) (**Figure 5a**), likely owing to poor signal-to-noise observed (**Figure 4c and 4d**). When looking at particle counts across the entirety of the peak within the ASTRA software, these erroneous counts greatly influence the total particle count. The sphere and Lorenz-Mie models show similar particle count; however, across the RI range of 1.35 to 1.65, a two order of magnitude change in particle counts is observed and is consistent between both OMV samples.

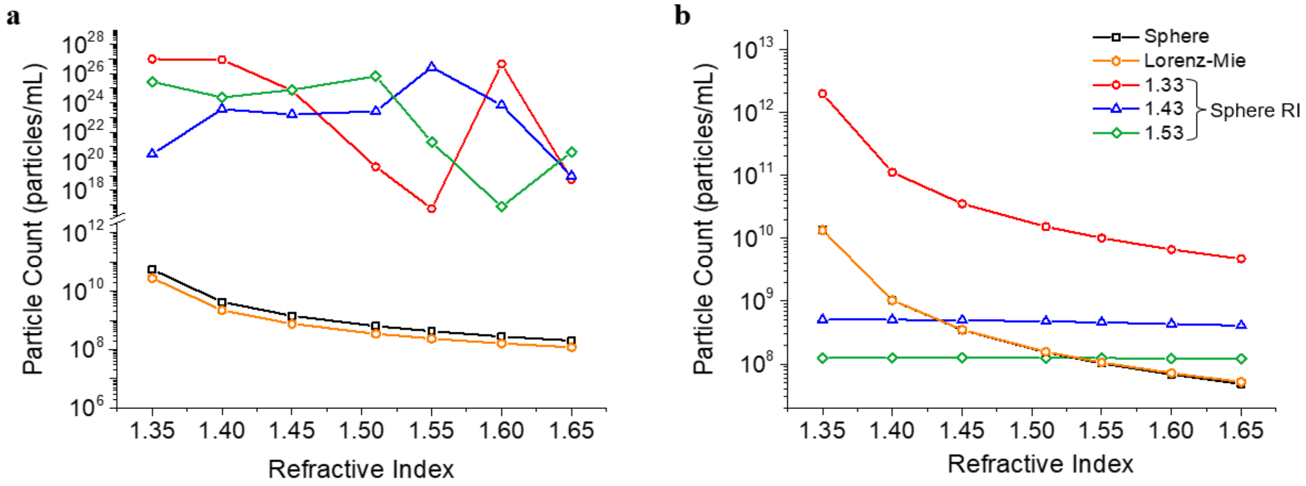

Figure 5. Effect of RI values and light scattering model on particle counts for results for (a) lignin-free and (b) lignin-rich samples. Light scattering models include sphere, Lorenz-Mie, and coated sphere. For the coated sphere model, the sphere RI value was kept constant at 1.33, 1.43, or 1.53 while the shell RI value (x-axis) was changed. The shell thickness was held constant at 6 nm. Data corresponds to fractograms shown in Figure 4c.

Unlike the lignin-free OMVs, the lignin-rich OMVs do not exhibit the higher particle counts for the coated sphere model (**Figure 5b**) likely as lignin-rich samples exhibited a much larger signal-to-noise ratio owing to larger particle size **(Figure 4e).** Instead, there is a trend where at low sphere RI values (1.33), the coated sphere model behaves similarly to the sphere and Lorenz-Mie model but gives rise to larger number of particles. With sphere RI values held constant 1.43 or 1.53, the particle counts are stabilized across the changing shell RI values and at a constant shell thickness. These trends hint at the sphere RI in the coated sphere model having a greater influence on particle counts. The difference in magnitude of the particle counts between sphere RI values of 1.43 and 1.53 can be attributed to the ratio of analyte and solvent refractive index that is seen in the single particle scattering function (i (θ), **Eq 2**). While this change in counts can be attributed to the sphere RI, this trend does not hold for the sphere RI of 1.33 and can be examined more closely via the shell RI and shell thickness. With respect to using the sphere model for the lignin-rich samples, the overall trend in counts matched those using the Lorenz-Mie model which is unexpected. Despite the upper size limit being lower than the sizes measured for the lignin-rich OMVs, the sphere model may not be showing major differences in particle counts due to the influence of detector selection as discussed earlier.

Impacts of Shell Thickness on OMV Particle Counts

As the sphere RI approaches or equals the RI value of the suspending fluid using the coated sphere model, particle counts appear to increase significantly (**Figure 5b, red trace**). Because this trend deviates from the higher sphere RI values, the shell thickness and RI values could be influencing the magnitude of the particle counts. When examining different shell thickness values of 2, 4, and 6 nm across the different sphere RI values, a sphere value of 1.33 shows significant variation in the magnitude of particle counts with respect to shell refractive index and shell thickness[51] (**Figure 6a**).

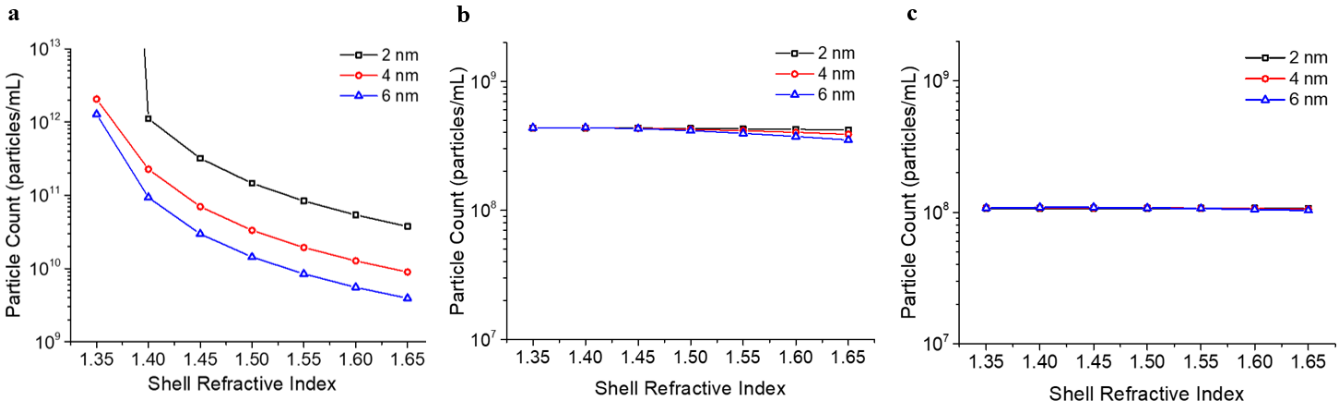

Figure 6. Effect of shell thickness on particle counts for the peak in the MALS fractogram of the lignin-rich samples using the coated sphere model. The sphere RI was kept constant at (a) 1.33, (b) 1.43, or (c) 1.53 while changing shell RI value. For each sphere and shell RI value combination, the particle counts were calculated for shell thicknesses of 2, 4, and 6 nm.

Based on the results from **Figures 5b and 5c,** it can be concluded that the counts are not affected by either the shell RI or thickness (**Figure 6b and 6c**). This reiterates the dominating parameter in the coated sphere model is the sphere RI. In the case of unknown shell thickness and RI values, there is more leniency in the estimation of shell thickness compared to sphere RI values. Despite being a better representation of the OMVs, the sensitivity of the coated sphere model does not allow accurate particle counting for the smaller OMVs due to the low signal-to-noise. Therefore, particle counts in lignin-free and lignin-rich media cannot be compared directly using this model.

CONCLUSIONS

This work presents an AF4-MALS method for the simultaneous separation and enumeration of polydisperse bioparticles, including bacterial OMVs. Key analyte-dependent parameters that impact MALS particle counts were identified to include light scattering theory/model, RI, and signal-to-noise ratio (S/N). Bioparticle counts via MALS was found to be most suitable when shape and RI are known, and good signal intensity at all angles is achieved. In sum, AF4-MALS can be used as a separation, enumeration, and purification method for bioparticles such as OMVs but relies on careful consideration of key MALS parameters.

The effect of light scattering theory was systematically evaluated for PSL standards and OMV bioparticles using sphere, Lorenz-Mie, and coated sphere models. Between the three spherical models studied, the coated sphere model is most sensitive to noise in the measured signal intensity; samples with S/N > 800 returned reasonable particle counts but were greatly influenced by the inner sphere RI. The sphere and Lorenz-Mie models are less sensitive to S/N, but a small RI range yields up to a 200% variation in OMV particle counts. Deviations between results from the sphere and Lorenz-Mie models can be attributed to assumptions within the light scattering theory and warrant special consideration when working with materials that strongly scatter light. To address this, improved model fits utilizing lower detector angles would provide more accurate particle counts for both sphere and Lorenz-Mie models. Moreover, the trends observed with PSL standards demonstrate appropriate and expected MALS responses, however only relative particle counts can be achieved. To determine absolute particle counts, a particle count standard with a closer refractive index to water (RI =1.33) would satisfy the assumptions made with the RGD approximation.

RI selection also greatly impacts particle counts regardless of model, and therefore should be carefully and independently considered for each bioparticle's analysis. While biochemical analyses can inform the compositional ratio of biological particles and aid in calculating an RI, this remains a time-intensive process and is not a standard practice in the field. Thus, new methods for RI determination of bioparticles could aid in improving the accuracy of MALS particle counts and could impact other data analyses such as DLS.

ACKNOWLEDGMENTS

This material is based upon work primarily supported by the National Science Foundation (NSF) under NSF Awards CHE-401438 and CHE-1808805 (CLP and SKRW) along with the Colorado School of Mines Undergraduate Research Fellowship (EB). This work was authored by the Alliance for Sustainable Energy, LLC, the manager and operator of the National Renewable Energy Laboratory for the U.S. Department of Energy (DOE), under Contract No. DE-AC36-08GO28308 (all authors). Funding was provided by The Center for Bioenergy Innovation a U.S. Department of Energy Research Center supported by the Office of Biological and Environmental Research in the DOE Office of Science. The views expressed herein do not necessarily represent the views of the DOE or the U.S. Government. The U.S. Government retains and the publisher, by accepting the article for publication, acknowledges that the U.S. Government retains a non-exclusive, paid-up, irrevocable, worldwide license to publish or reproduce the published form of this work, or allow others to do so, for U.S. Government purposes. The authors would also like thank Wyatt Technology Corporation for the customer service support and suggestions.

SUPPORTING INFORMATION

AF4 method development using polystyrene latex, impacts of detector selection for polystyrene latex particles, table with literature dn/dc and RI values for OMV components, and detector number and corresponding angles for MALS instrumentation (PDF).

REFERENCES

(1) Maia, J.; Caja, S.; Moraes, M. C. S.; Couto, N.; Costa-Silva, B. Exosome- Based Cell-Cell Communication in the Tumor Microenvironment. *Front Cell Dev Biol* **2018**, *6*.

(2) Ziegenbalg, A.; Prados-Rosales, R.; Jenny-Avital, E. R.; Kim, R. S.; Casadevall, A.; Achkar, J. M. Immunogenicity of Mycobacterial Vesicles in Humans: Identification of a

New Tuberculosis Antibody Biomarker. *Tuberculosis* **2013**, *93*, 448–455. https://doi.org/10.1016/j.tube.2013.03.001.

(3) Ciferri, M. C.; Quarto, R.; Tasso, R.; Bernardi, S. Extracellular Vesicles as Biomarkers and Therapeutic Tools: From Pre-Clinical to Clinical Applications. *Biology (Basel)* **2021**, *10*, 359. https://doi.org/10.3390/biology.

(4) Suntres, Z. E.; Smith, M. G.; Momen-Heravi, F.; Hu, J.; Zhang, X.; Wu, Y.; Zhu, H.; Wang, J.; Zhou, J.; Kuo, W. P. Therapeutic Uses of Exosomes. *J Circ Biomark* **2013**, *1*, 1. https://doi.org/10.5772/56522.

(5) Vogel, R.; Savage, J.; Muzard, J.; Camera, G. Della; Vella, G.; Law, A.; Marchioni, M.; Mehn, D.; Geiss, O.; Peacock, B.; Aubert, D.; Calzolai, L.; Caputo, F.; Prina-Mello, A. Measuring Particle Concentration of Multimodal Synthetic Reference Materials and Extracellular Vesicles with Orthogonal Techniques: Who Is up to the Challenge? *J Extracell Vesicles* **2021**, *10* (3). https://doi.org/10.1002/jev2.12052.

(6) Coumans, F. A. W.; Van Der Pol, E.; Böing, A. N.; Hajji, N.; Sturk, G.; Van Leeuwen, T. G.; Nieuwland, R.; Bö Ing, A. N. Reproducible Extracellular Vesicle Size and Concentration Determination with Tunable Resistive Pulse Sensing. *J Extracell Vesicles* **2014**, *3* (25922). https://doi.org/10.3402/jev.v3.25922.

(7) Péter, P.; Terejánszky, T.; Makra, I. I.; Fü, P. P.; Róbert, R.; Gyurcsányigyurcsányi, E. Calibration-Less Sizing and Quantitation of Polymeric Nanoparticles and Viruses with Quartz Nanopipets. **2014**. https://doi.org/10.1021/ac500184z.

(8) Makra, I.; Terejánszky, P.; Gyurcsányi, R. E. A Method Based on Light Scattering to Estimate the Concentration of Virus Particles without the Need for Virus Particle Standards. *MethodsX* **2015**. https://doi.org/10.1016/j.mex.2015.02.003.

(9) Filipe, V.; Hawe, A.; Jiskoot, W. Critical Evaluation of Nanoparticle Tracking Analysis (NTA) by NanoSight for the Measurement of Nanoparticles and Protein Aggregates. *Pharm Res* **2010**, *27* (5), 796–810. https://doi.org/10.1007/s11095-010-0073-2.

(10) Wei, Z.; McEvoy, M.; Razinkov, V.; Polozova, A.; Li, E.; Casas-Finet, J.; Tous, G. I.; Balu, P.; Pan, A. A.; Mehta, H.; Schenerman, M. A. Biophysical Characterization of Influenza Virus Subpopulations Using Field Flow Fractionation and Multiangle Light Scattering: Correlation of Particle Counts, Size Distribution and Infectivity. *J Virol Methods* **2007**, *144* (1–2), 122–132. https://doi.org/10.1016/j.jviromet.2007.04.008.

(11) Adkins, G. B.; Sun, E.; Coreas, R.; Zhong, W. Asymmetrical Flow Field Flow Fractionation Coupled to Nanoparticle Tracking Analysis for Rapid Online Characterization of Nanomaterials. *Anal Chem* **2020**, *92*, 7071–7078. https://doi.org/10.1021/acs.analchem.0c00406.

(12) Sitar, S.; Kejž, A.; Pahovnik, D.; Kogej, K.; Tuš Ek-Z, M.; Nidarič,ˇ; Lenassi, M.; Agar, E. Z.ˇ. Size Characterization and Quantification of Exosomes by Asymmetrical-Flow Field-Flow Fractionation. **2015**. https://doi.org/10.1021/acs.analchem.5b01636.

(13) Parot, J.; Mehn, D.; Jankevics, H.; Markova, N.; Carboni, M.; Olaisen, C.; Hoel, A. D.; Sigfúsdóttir, M. S.; Meier, F.; Drexel, R.; Vella, G.; McDonagh, B.; Hansen, T.; Bui, H.; Klinkenberg, G.; Visnes, T.; Gioria, S.; Urban-Lopez, P.; Prina-Mello, A.; Borgos, S. E.; Caputo, F.; Calzolai, L. Quality Assessment of LNP-RNA Therapeutics with Orthogonal Analytical Techniques. *Journal of Controlled Release* **2024**, *367*, 385–401. https://doi.org/10.1016/j.jconrel.2024.01.037.

(14) Gardiner, C.; Ferreira, Y. J.; Dragovic, R. A.; Redman, C. W. G.; Sargent, I. L. Extracellular Vesicle Sizing and Enumeration by Nanoparticle Tracking Analysis. *J Extracell Vesicles* **2013**, *2* (1). https://doi.org/10.3402/jev.v2i0.19671.

(15) Bachurski, D.; Schuldner, M.; Nguyen, P.-H.; Malz, A.; Reiners, K. S.; Grenzi, P. C.; Babatz, F.; Schauss, A. C.; Hansen, H. P.; Hallek, M.; Pogge, E.; Strandmann, V. Extracellular Vesicle Measurements with Nanoparticle Tracking Analysis – An Accuracy and Repeatability Comparison between NanoSight NS300 and ZetaView. *J Extracell Vesicles* **2019**, *8*. https://doi.org/10.1080/20013078.2019.1596016.

(16) Andersson, M.; Wittgren, B.; Wahlund, K. G. Accuracy in Multiangle Light Scattering Measurements for Molar Mass and Radius Estimations. Model Calculations and Experiments. *Anal Chem* **2003**, *75* (16), 4279–4291. https://doi.org/10.1021/ac030128+.

(17) Gao, W.; Cohen, J.; Acholla, F.; Su, W. Development of Asymmetrical Flow Field Fractionation with On-Line Advanced Detections for Particle Size Distribution Analysis of Silica Colloidal Particles. *ACS Symposium Series* **2018**, *1281*, 111–143. https://doi.org/10.1021/bk-2018-1281.ch007.

(18) Mildner, R.; Hak, S.; Parot, J.; Hyldbakk, A.; Borgos, S. E.; Some, D.; Johann, C.; Caputo, F. Improved Multidetector Asymmetrical-Flow Field-Flow Fractionation Method for Particle Sizing and Concentration Measurements of Lipid-Based Nanocarriers for RNA Delivery. *European Journal of Pharmaceutics and Biopharmaceutics* **2021**. https://doi.org/10.1016/j.ejpb.2021.03.004.

(19) Parupudi, A.; Gruia, F.; Korman, S. A.; Dragulin-Otto, S.; Sra, K.; Remmele, R. L.; Bee, J. S. Biophysical Characterization of Influenza A Virions. *J Virol Methods* **2017**, *247*, 91–98. https://doi.org/10.1016/j.jviromet.2017.06.002.

(20) Zhang, H.; Lyden, D. Asymmetric-Flow Field-Flow Fractionation Technology for Exomere and Small Extracellular Vesicle Separation and Characterization. *Nat Protoc* **2019**, *14* (4), 1027–1053. https://doi.org/10.1038/s41596-019-0126-x.

(21) Zhang, H.; Freitas, D.; Kim, H. S.; Fabijanic, K.; Li, Z.; Chen, H.; Mark, M. T.; Molina, H.; Martin, A. B.; Bojmar, L.; Fang, J.; Rampersaud, S.; Hoshino, A.; Matei, I.; Kenific, C. M.; Nakajima, M.; Mutvei, A. P.; Sansone, P.; Buehring, W.; Wang, H.; Jimenez, J. P.; Cohen-Gould, L.; Paknejad, N.; Brendel, M.; Manova-Todorova, K.; Magalhães, A.; Ferreira, J. A.; Osório, H.; Silva, A. M.; Massey, A.; Cubillos-Ruiz, J. R.; Galletti, G.; Giannakakou, P.; Cuervo, A. M.; Blenis, J.; Schwartz, R.; Brady, M. S.; Peinado, H.; Bromberg, J.; Matsui, H.; Reis, C. A.; Lyden, D. Identification of Distinct Nanoparticles and Subsets of Extracellular Vesicles by Asymmetric Flow Field-Flow Fractionation. *Nat Cell Biol* **2018**, *20* (3), 332–343. https://doi.org/10.1038/s41556-018-0040-4.

(22) van der Put, R. M. F.; Spies, A.; Metz, B.; Some, D.; Scherrers, R.; Pieters, R.; Danial, M. Validation of an FFF-MALS Method to Characterize the Production and Functionalization of Outer-Membrane Vesicles for Conjugate Vaccines. *Anal Chem* **2022**, *94*, 12033–12041. https://doi.org/10.1021/acs.analchem.2c01590.

(23) Steppert, P.; Burgstaller, D.; Klausberger, M.; Tover, A.; Berger, E.; Jungbauer, A. Quantification and Characterization of Virus-like Particles by Size-Exclusion Chromatography and Nanoparticle Tracking Analysis. *J Chromatogr A* **2017**, *1487*, 89–99. https://doi.org/10.1016/j.chroma.2016.12.085.

(24) Dell'annunziata, F.; Folliero, V.; Giugliano, R.; De Filippis, A.; Santarcangelo, C.; Izzo, V.; Daglia, M.; Galdiero, M.; Arciola, C. R.; Franci, G.; Belén Flórez, A. Molecular Sciences Gene Transfer Potential of Outer Membrane Vesicles of Gram-Negative Bacteria. *Int J Mol Sci* **2021**, 5985. https://doi.org/10.3390/ijms.

(25) Reimer, S. L.; Beniac, D. R.; Hiebert, S. L.; Booth, T. F.; Chong, P. M.; Westmacott, G. R.; Zhanel, G. G.; Bay, D. C. Comparative Analysis of Outer Membrane Vesicle Isolation Methods With an Escherichia Coli TolA Mutant Reveals a Hypervesiculating Phenotype With Outer-Inner Membrane Vesicle Content. *Front Microbiol* **2021**, *12*. https://doi.org/10.3389/fmicb.2021.628801.

(26) Schwechheimer, C.; Kuehn, M. J. Outer-Membrane Vesicles from Gram-Negative Bacteria: Biogenesis and Functions. *Nature Reviews Microbiology*. Nature Publishing Group September 16, 2015, pp 605–619. https://doi.org/10.1038/nrmicro3525.

(27) Nagakubo, T.; Nomura, N.; Toyofuku, M. Cracking Open Bacterial Membrane Vesicles. *Front Microbiol* **2020**, *10* (January), 1–9. https://doi.org/10.3389/fmicb.2019.03026.

(28) Maxwell, J. C. A Dynamical Theory of the Electromagnetic Field. *Philosophical Transactions Royal Society* **1865**, *155*, 459–512.

(29) Rayleigh F.R.S., Lord. XXXIV On the Transmission of Light through an Atmosphere Containing Small Particles in Suspension and the Origin of the Blue of the Sky. *The*

London, Edinburgh, and Dublin Philosophical Magazine and Journal of Science. **1899**, *47* (287), 375–384.

(30) Rayleigh F.R.S, Lord. X. On the Electromagnetic Theory of Light . *The London, Edinburgh, and Dublin Philosophical Magazine and Journal of Science* **1881**, *12* (73), 81–101. https://doi.org/10.1080/14786448108627074.

(31) Mie, G. Beiträge Zur Optik Trüber Medien, Speziell Kolloidaler Metallösungen. *Ann Phys* **1908**, *330* (3), 377–445. https://doi.org/10.1002/andp.19083300302.

(32) van de Hulst, H. C. *Light Scattering by Small Particles*; John Wiley and Sons: New York, 1957.

(33) Kerker, M. *The Scattering of Light and Other Electromagnetic Radiation*; Academic Press: New York, 1969.

(34) Technology Corporation, W. *DAWN® User's Guide*; 2020.

(35) Wyatt, P. J.; Weida, M. J. Method and Apparatus for Determining Absolute Number Densities of Particles in Solution. US 6,774,994 B1, 2004.

(36) Lockwood, D. J. Rayleigh and Mie Scattering. *Encyclopedia of Color Science and Technology*; Springer New York, 2016; pp 1097–1107. https://doi.org/10.1007/978-1-4419-8071-7.

(37) Wyatt, P. J. Measurement of Special Nanoparticle Structures by Light Scattering. *Analytical Chemistry*. American Chemical Society August 5, 2014, pp 7171–7183. https://doi.org/10.1021/ac500185w.

(38) Salvachúa, D.; Werner, A. Z.; Pardo, I.; Michalska, M.; Black, B. A.; Donohoe, B. S.; Haugen, S. J.; Katahira, R.; Notonier, S.; Ramirez, K. J.; Amore, A.; Purvine, S. O.; Zink, E. M.; Abraham, P. E.; Giannone, R. J.; Poudel, S.; Laible, P. D.; Hettich, R. L.; Beckham, G. T. Outer Membrane Vesicles Catabolize Lignin-Derived Aromatic Compounds in Pseudomonas Putida KT2440. *PNAS* **2020**, 1–9. https://doi.org/10.1073/pnas.1921073117.

(39) Linger, J. G.; Vardon, D. R.; Guarnieri, M. T.; Karp, E. M.; Hunsinger, G. B.; Franden, M. A.; Johnson, C. W.; Chupka, G.; Strathmann, T. J.; Pienkos, P. T.; Beckham, G. T. Lignin Valorization through Integrated Biological Funneling and Chemical Catalysis. https://doi.org/10.1073/pnas.1410657111.

(40) Leeman, M.; Choi, J.; Hansson, S.; Storm, M. U.; Nilsson, L. Proteins and Antibodies in Serum, Plasma, and Whole Blood-Size Characterization Using Asymmetrical Flow Field-Flow Fractionation (AF4). https://doi.org/10.1007/s00216-018-1127-2.

(41) Gao, Z.; Hutchins, Z.; Li, Z.; Zhong, W. Offline Coupling of Asymmetrical Flow Field-Flow Fractionation and Capillary Electrophoresis for Separation of Extracellular Vesicles. **2022**. https://doi.org/10.1021/acs.analchem.2c03550.

(42) Caputo, F.; Vogel, R.; Savage, J.; Vella, G.; Law, A.; Della Camera, G.; Hannon, G.; Peacock, B.; Mehn, D.; Ponti, J.; Geiss, O.; Aubert, D.; Prina-Mello, A.; Calzolai, L. Measuring Particle Size Distribution and Mass Concentration of Nanoplastics and Microplastics: Addressing Some Analytical Challenges in the Sub-Micron Size Range. *J Colloid Interface Sci* **2021**, *588*, 401–417. https://doi.org/10.1016/j.jcis.2020.12.039.

(43) McEvoy, M.; Razinkov, V.; Wei, Z.; Casas-finet, J. R.; Tous, G. I.; Schenerman, M. A. Improved Particle Counting and Size Distribution Determination of Aggregated Virus Populations by Asymmetric Flow Field-Flow Fractionation and Multiangle Light Scattering Techniques. **2011**, 547–554. https://doi.org/10.1002/btpr.499.

(44) Welsh, J. A.; Pol, E. van der; Bettin, B. A.; Carter, D. R. F.; Hendrix, A.; Lenassi, M. Towards Defining Reference Materials for Measuring Extracellular Vesicle Refractive Index , Epitope Abundance , Size and Concentration. *J Extracell Vesicles* **2020**, *9* (1). https://doi.org/10.1080/20013078.2020.1816641.

(45) Ramirez, M. I.; Amorim, M. G.; Gadelha, C.; Milic, I.; Welsh, J. A.; Freitas, V. M.; Nawaz, M.; Akbar, N.; Couch, Y.; Makin, L.; Cooke, F.; Vettore, A. L.; Batista, P. X.; Freezor, R.; Pezuk, J. A.; Rosa-Fernandes, L.; Carreira, A. C. O.; Devitt, A.; Jacobs, L.; Silva, I. T.; Coakley, G.; Nunes, D. N.; Carter, D.; Palmisano, G.; Dias-Neto, E. Technical Challenges of Working with Extracellular Vesicles. *Nanoscale* **2018**, *10* (3), 881–906. https://doi.org/10.1039/c7nr08360b.

(46) van der Pol, E.; Coumans, F. A. W.; Grootemaat, A. E.; Gardiner, C.; Sargent, I. L.; Harrison, P.; Sturk, A.; van Leeuwen, T. G.; Nieuwland, R. Particle Size Distribution of Exosomes and Microvesicles Determined by Transmission Electron Microscopy, Flow Cytometry, Nanoparticle Tracking Analysis, and Resistive Pulse Sensing. *Journal of Thrombosis and Haemostasis* **2014**, *12* (7), 1182–1192. https://doi.org/10.1111/jth.12602.

(47) Gardiner, C.; Shaw, M.; Hole, P.; Smith, J.; Tannetta, D.; Redman, C. W.; Sargent, I. L. Measurement of Refractive Index by Nanoparticle Tracking Analysis Reveals Heterogeneity in Extracellular Vesicles. *J Extracell Vesicles* **2014**, *3* (25361), 1–6. https://doi.org/10.3402/jev.v3.25361.

(48) Pol, E. Van Der; Rond, L. De; Coumans, F. A. W.; Gool, E. L.; Böing, A. N.; Sturk, A.; Nieuwland, R. Absolute Sizing and Label-Free Identification of Extracellular Vesicles by Flow Cytometry LPs EVs. *Nanomedicine* **2018**, *14* (3), 801–810. https://doi.org/10.1016/j.nano.2017.12.012.

(49) Geeurickx, E.; Tulkens, J.; Dhondt, B.; Deun, J. Van; Lippens, L.; Vergauwen, G.; Heyrman, E.; Sutter, D. De; Gevaert, K.; Impens, F.; Miinalainen, I.; Bockstal, P. Van; Beer, T. De; Wauben, M. H. M.; Nieuwland, R.; Braems, G.; Callewaert, N.; Mestdagh, P.; Vandesompele, J. The Generation and Use of Recombinant Extracellular Vesicles as Biological Reference Material. *Nat Commun* **2019**, *10*, 3288–3298. https://doi.org/10.1038/s41467-019-11182-0.

(50) Rond, L. De; Libregts, S. F. W. M.; Rikkert, L. G.; Hau, C. M.; Pol, E. Van Der; Nieuwland, R.; Leeuwen, T. G. Van. Refractive Index to Evaluate Staining Specificity of Extracellular Vesicles by Flow Cytometry. *J Extracell Vesicles* **2019**, *8* (1). https://doi.org/10.1080/20013078.2019.1643671.

(51) Santos, N. C.; Silva, A. C.; Castanho, M. A. R. B.; Martins-silva, J.; Saldanha, C. Evaluation of Lipopolysaccharide Aggregation by Light Scattering Spectroscopy. **2003**, 96–100.